On the onset of convection in a highly–permeable vertical porous layer with open boundaries

A. Barletta[1, a)] and D.A.S. Rees[2, b)]

[1)]*Department of Industrial Engineering, Alma Mater Studiorum Università di Bologna,*
Viale Risorgimento 2, 40136 Bologna, Italy
[2)]*Department of Mechanical Engineering, University of Bath,*
Claverton Down, Bath BA2 7AY, UK

The unstable nature of buoyant flow in a vertical porous slab with a pure conduction temperature distribution is investigated. The permeable and isothermal boundaries are subject to a temperature difference, which is responsible for the basic stationary and parallel vertical flow in the slab. The momentum transfer is modelled by adopting the Darcy–Forchheimer law, thus including the quadratic form–drag contribution. The instability to small–amplitude perturbations is tested by parametrising the basic stationary flow through the Darcy–Rayleigh number and the form–drag number. The modal analysis is carried out numerically with a pressure–temperature formulation of the governing equations for the perturbations. The neutral stability curves and the critical values of the wave number and the Darcy–Rayleigh number are obtained for different prescribed values of the form–drag number.

I. INTRODUCTION

Highly–permeable porous materials deserve a widespread interest from the engineering community due to their role in the intensification of heat transfer processes. The main example is metal foams which are considered by several authors as a possible alternative to micro–finned surfaces in the design of compact heat exchangers[1]. The main characteristic of porous media with a large value of permeability is the departure from Darcy's law in the modelling of momentum transfer, with the emergence of a quadratic form-drag effect[2].

The natural convection in a vertical porous slab may display a stationary parallel flow regime where the temperature varies linearly across the slab. In this regime, heat transfer is not influenced by the buoyant flow and displays the same features of pure heat conduction. The possibility of breaking this conduction regime by the onset of a thermal instability and the development of a multicellular convection flow was ruled out by Gill[3]. This author presented a very elegant proof that the conduction regime in the vertical porous slab is always linearly stable. Straughan[4] and Flavin and Rionero[5] were able to show that stability is ensured also if the assumption of linearity is relaxed.

Gill's stability theorem[3] strongly relies on the boundary conditions imposed at the vertical boundaries of the porous slab. In particular, it is quite important that the boundaries are impermeable. Barletta[6] proved that an instability of the conduction regime can be developed for sufficiently large values of the Darcy–Rayleigh number provided that the boundaries are permeable.

There is an intrinsic interest in the findings reported above, due to the chance of investigating a thermal instability mechanism that differs from the usual Rayleigh–Bénard phenomenon. In fact, the instability detected by Barletta[6] is not

triggered by heating from below, but by side heating. In this respect, the scenario is very similar to that considered by Vest and Arpaci[7], Korpela, Gözüm, and Baxi[8], and McBain and Armfield[9] having in mind the case of a fluid, instead of a fluid saturated porous medium. Besides the theoretical aspects, the possible onset of multicellular flow in a vertical porous layer is closely connected to engineering applications such as the breathing walls employed in the building industry[10], or the thermal control of groundwater reservoirs, or the diffusion of pollutants from underground nuclear waste repositories.

The results regarding the possible instability of a vertical porous slab with permeable boundaries reported by Barletta[6] were further developed by considering the lack of local thermal equilibrium between the solid and the fluid[11,12], as well as imperfectly conducting boundaries modelled through Robin conditions for the temperature[13]. Other recent papers on this topic investigated other aspects of the onset of instability in a vertical porous layer saturated by a fluid[14–21].

The aim of this study is to further develop the knowledge of this topic by generalising the results obtained adopting Darcy's law to cases where the very large porosity (*e.g.* the metal foams employed for compact heat exchangers) may justify the inclusion of the quadratic form–drag term in the momentum balance for the saturated medium. This aspect of the instability in a vertical porous layer has not yet been investigated in the existing literature. The system setup is just the same as that devised in the study by Barletta[6], namely a vertical porous slab with infinite height bounded by isothermal open boundaries. The dynamics of the linear perturbations acting on the basic stationary and parallel flow is constrained by zero temperature and pressure boundary conditions. A convective instability is developed when the Darcy–Rayleigh number, proportional to the temperature difference imposed between the boundaries, exceeds its critical value. The critical value depends on an additional dimensionless parameter measuring the discrepancy from Darcy's law behaviour, the form–drag number. Through a numerical solution of the stability eigenvalue problem, it is shown that a departure from the Darcy's law regime means stabilisation. This outcome is ex-

---

[a)]Electronic mail: antonio.barletta@unibo.it
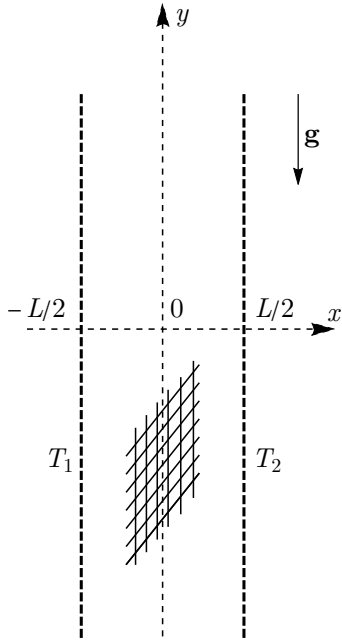[b)]Electronic mail: D.A.S.Rees@bath.ac.uk

FIG. 1. Two-dimensional sketch of the vertical porous slab

pected by analogy with what was found by Rees [22] regarding the onset of instability in a horizontal porous layer with an imposed uniform flow and heating from below. We mention that a similar feature has been recently pointed out also by Barletta and Rees [23] while studying the instability of mixed convection in a horizontal porous channel with uniformly heated walls.

II. MATHEMATICAL MODEL

The momentum balance in the saturated porous medium is modelled through the Darcy–Forchheimer law [2],

$$\frac{\mu}{K}\left(1 + c_F \frac{|\mathbf{u}|\sqrt{K}}{\nu}\right)\mathbf{u} = -\boldsymbol{\nabla}P - \rho\,\gamma(T - T_0)\,\mathbf{g}, \quad (1)$$

where the buoyancy force is included alongside the pressure gradient term. More precisely, P denotes the local difference between the pressure and the hydrostatic pressure as prescribed when applying the Oberbeck–Boussinesq approximation for convective flow. The term proportional to c_F yields the quadratic form–drag whose magnitude marks the departure from Darcy's law. In Eq. (1), $\mathbf{u} = (u, v, w)$ is the velocity, T is the temperature, T_0 is the reference temperature, μ is the dynamic viscosity, ν is the kinematic viscosity, ρ is the fluid density, K is the permeability, c_F is the form–drag parameter, γ is the thermal expansion coefficient of the fluid, and $\mathbf{g}$ is the gravitational acceleration whose modulus is g.

As displayed in Fig. 1, we are considering a vertical porous slab with thickness L, bounded by isothermal permeable surfaces with temperatures T_1 and T_2. The sketch in Fig. 1 is two–dimensional. The horizontal coordinate x spans the limited interval $[-L/2, L/2]$, while the horizontal unbounded co-

ordinate z, not visible in the figure, varies over all possible real values. The vertical coordinate y is unbounded as well and defines the direction of the basic buoyant flow along the slab. The $y-$axis is parallel to the gravitational acceleration $\mathbf{g}$, but with opposite direction so that $\mathbf{g} = -g\,\mathbf{e}_y$. A dimensionless expression of the governing equations, given by the local mass balance, the local momentum balance, $viz.$ Eq. (1), and the local energy balance can be formulated as

$$\boldsymbol{\nabla}\cdot\mathbf{u} = 0, \qquad (2a)$$

$$(1 + \xi|\mathbf{u}|)\,\mathbf{u} = -\boldsymbol{\nabla}P + T\mathbf{e}_y, \qquad (2b)$$

$$\frac{\partial T}{\partial t} + \mathbf{u}\cdot\boldsymbol{\nabla}T = \nabla^2 T. \qquad (2c)$$

We have, in fact, employed the scaling

$$(x,y,z)\frac{1}{L} \to (x,y,z), \qquad t\,\frac{\lambda}{\sigma L^2} \to t,$$

$$(u,v,w)\frac{L}{\lambda} \to (u,v,w),$$

$$P\frac{K}{\mu\lambda} \to P, \qquad (T - T_0)\frac{g\gamma KL}{\nu\lambda} \to T, \qquad (3)$$

to define the dimensionless coordinates, time and fields. We mention that the time scaling introduced in Eq. (3) involves the average thermal diffusivity, λ, as well as the dimensionless ratio, σ, between the volumetric heat capacity of the saturated medium and that of the fluid [2]. The dimensionless scaling is completed by the definition of the Darcy–Rayleigh number and the form–drag number,

$$R = \frac{g\gamma(T_2 - T_1)KL}{\nu\lambda}, \qquad \xi = \frac{c_f\lambda\sqrt{K}}{\nu L}. \qquad (4)$$

The Darcy–Rayleigh number extends the meaning of the Rayleigh number for fluids in the absence of a porous matrix. Its value determines the strength of the buoyancy–induced convection flow. The form–drag number measures the importance of the Forchheimer quadratic term in the local momentum balance relative to the Darcy linear term.

As pointed out in the literature (see, for example, Nield and Bejan [2]), the emergence of important form–drag effects does not depend only on the permeability. Most authors [2], in fact, assume that the transition from the Darcy regime to the Forchheimer regime happens when the *permeability–based* Reynolds number,

$$Re_K = \frac{|\mathbf{u}|\sqrt{K}}{\nu}, \qquad (5)$$

lies in the range $1 \le Re_K \le 10$. According to this criterion, obviously the permeability must be large enough for the transition to occur, but how large it has to be depends on the maximum velocity in the flow domain and on the fluid viscosity.

The formulation of the problem sketched in Fig. 1 leads to the dimensionless boundary conditions,

$$x = \pm 1/2: \qquad P = 0, \qquad T = \pm\frac{R}{2}. \qquad (6)$$

We point out that a vanishing boundary value of P means that a continuous transition at $x = \pm 1/2$ happens between the internal distribution of P within the porous slab and the hydrostatic pressure in quiescent fluid reservoirs adjacent to the external boundaries, as described in Barletta[6].

III. THE BASIC PARALLEL FLOW

Equations (2) and (6) admit a stationary solution describing parallel buoyancy–driven flow in the slab,

$$u_b = 0, \quad v_b = \frac{2Rx}{1 + \sqrt{4R\xi \, |x| + 1}}, \quad w_b = 0,$$
$$T_b = Rx, \quad P_b = 0, \tag{7}$$

where b serves to denote "basic flow". The flow given by Eq. (7) is directed along the vertical $y-$axis and its orientation is downward for $-1/2 < x < 0$ and upward for $0 < x < 1/2$. One may evaluate the mean value of v in the half–slab with $0 < x < 1/2$,

$$v_{bm} = \frac{(1+2R\xi)^{3/2} - 3R\xi - 1}{6R\xi^2} = \frac{R}{3} \frac{1 + 2\sqrt{1+2R\xi}}{(1 + \sqrt{1+2R\xi})^2}. \tag{8}$$

As the velocity profile is an odd function of x, $-v_{bm}$ yields the mean value of v in the half–slab with $-1/2 < x < 0$. By taking the limit $\xi \to 0$, one recovers the basic solution implied by Darcy's law, namely that studied by both Gill[3] and Barletta[6]. In particular, in this limit, one has $v_{bm} = R/4$.

Figure 2(a) displays the basic velocity profiles relative to $R = 200$ and different values of ξ, while Fig. 2(b) shows the decreasing trend of v_{bm} versus ξ for different values of R. Generally speaking, Fig. 2 reveals that the quadratic form–drag causes a change in the linear velocity profile, characteristic of the Darcy's flow solution, and leads to a gradual inhibition of the buoyant flow as ξ increases. This physical effect has a mathematical counterpart given by the denominator in the expression of v_b, Eq. (7), whose value for $x \neq 0$ increases when the form–drag becomes more and more intense.

IV. LINEAR STABILITY ANALYSIS

The dynamics of small-amplitude perturbations acting on the basic flow, Eq. (4), can be studied by substituting the expressions,

$$\mathbf{u} = \mathbf{u}_b + \varepsilon \, \tilde{\mathbf{u}}, \qquad T = T_b + \varepsilon \, \tilde{T}, \qquad P = P_b + \varepsilon \, \tilde{P}, \tag{9}$$

into Eqs. (2) and (6). Here ε represents a small perturbations parameter, so that all terms of $O(\varepsilon^2)$ or higher are negligible. This leads to the linearised stability equations and boundary conditions, namely

$$\frac{\partial \tilde{u}}{\partial x} + \frac{\partial \tilde{v}}{\partial y} + \frac{\partial \tilde{w}}{\partial z} = 0, \tag{10a}$$

$$(1 + \xi |v_b|) \, \tilde{u} = -\frac{\partial \tilde{P}}{\partial x}, \tag{10b}$$

$$(1 + 2\xi |v_b|) \, \tilde{v} = -\frac{\partial \tilde{P}}{\partial y} + \tilde{T}, \tag{10c}$$

$$(1 + \xi |v_b|) \, \tilde{w} = -\frac{\partial \tilde{P}}{\partial z}, \tag{10d}$$

$$\frac{\partial \tilde{T}}{\partial t} + R\tilde{u} + v_b \frac{\partial \tilde{T}}{\partial y} = \frac{\partial^2 \tilde{T}}{\partial x^2} + \frac{\partial^2 \tilde{T}}{\partial y^2} + \frac{\partial^2 \tilde{T}}{\partial z^2}, \tag{10e}$$

$$x = \pm 1/2: \qquad \tilde{P} = 0, \qquad \tilde{T} = 0. \tag{10f}$$

The perturbation velocity $\tilde{\mathbf{u}} = (\tilde{u}, \tilde{v}, \tilde{w})$, temperature $\tilde{T}$ and pressure $\tilde{P}$ are in fact determined by solving Eqs. (10).

We mention that, in order to obtain the linearised governing equations (10), the Forchheimer term, $\xi |\mathbf{u}| \mathbf{u}$, is rewritten by employing Eq. (9), so that it reads

$$\xi |\mathbf{u}| u =$$
$$\xi (u_b + \varepsilon \tilde{u}) \sqrt{(u_b + \varepsilon \tilde{u})^2 + (v_b + \varepsilon \tilde{v})^2 + (w_b + \varepsilon \tilde{w})^2}, \tag{11}$$

$$\xi |\mathbf{u}| v =$$
$$\xi (v_b + \varepsilon \tilde{v}) \sqrt{(u_b + \varepsilon \tilde{u})^2 + (v_b + \varepsilon \tilde{v})^2 + (w_b + \varepsilon \tilde{w})^2}, \tag{12}$$

$$\xi |\mathbf{u}| w =$$
$$\xi (w_b + \varepsilon \tilde{w}) \sqrt{(u_b + \varepsilon \tilde{u})^2 + (v_b + \varepsilon \tilde{v})^2 + (w_b + \varepsilon \tilde{w})^2}. \tag{13}$$

The right hand sides of these equations are intended as functions of ε. Then, we have just to write series expansions with respect to ε starting from $\varepsilon = 0$. Keeping in mind that in our case $u_b = 0 = w_b$, we obtain

$$\xi |\mathbf{u}| u = \xi \varepsilon \tilde{u} |v_b| + O(\varepsilon^2), \tag{14}$$

$$\xi |\mathbf{u}| v = \xi v_b |v_b| + 2 \xi \varepsilon \tilde{v} |v_b| + O(\varepsilon^2),$$

$$\xi |\mathbf{u}| w = \xi \varepsilon \tilde{w} |v_b| + O(\varepsilon^2).$$

By neglecting the terms $O(\varepsilon^2)$, we obtain the linearisation employed in Eqs. (9).

The governing equations (10) for stability can be rewritten by adopting a pressure–temperature formulation,

$$\frac{\partial}{\partial x} \left[(1 + \xi |v_b|)^{-1} \frac{\partial \tilde{P}}{\partial x} \right] + (1 + 2\xi |v_b|)^{-1} \frac{\partial^2 \tilde{P}}{\partial y^2}$$
$$+ (1 + \xi |v_b|)^{-1} \frac{\partial^2 \tilde{P}}{\partial z^2}$$
$$- (1 + 2\xi |v_b|)^{-1} \frac{\partial \tilde{T}}{\partial y} = 0, \tag{15a}$$

$$\frac{\partial \tilde{T}}{\partial t} - R (1 + \xi |v_b|)^{-1} \frac{\partial \tilde{P}}{\partial x} + v_b \frac{\partial \tilde{T}}{\partial y}$$
$$= \frac{\partial^2 \tilde{T}}{\partial x^2} + \frac{\partial^2 \tilde{T}}{\partial y^2} + \frac{\partial^2 \tilde{T}}{\partial z^2}, \tag{15b}$$

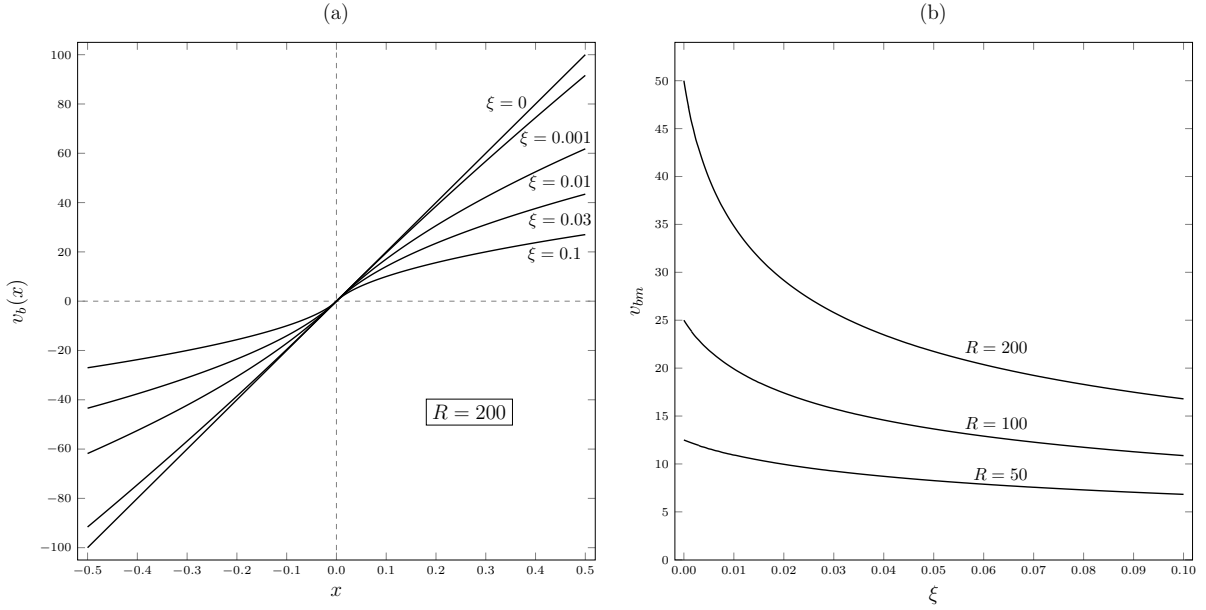$$x = \pm 1/2: \qquad \tilde{P} = 0, \qquad \tilde{T} = 0, \tag{15c}$$

FIG. 2. Basic solution: (a) velocity profiles, $v_b(x)$, for $R = 200$ relative to different ξ; (b) mean value, v_{bm}, of the basic velocity across the half-slab $0 < x < 1/2$ versus ξ with different Darcy–Rayleigh numbers, R

so that, now, the unknowns are just $\tilde{T}$ and $\tilde{P}$. Equation (15a) has been obtained by solving Eqs. (10b)–(10d) for $\tilde{u}$, $\tilde{v}$ and $\tilde{w}$ and then by employing Eq. (10a). A normal mode analysis can be applied with $\tilde{T}$ and $\tilde{P}$ given by

$$\tilde{T} = h(x)\, e^{i(\alpha y + \beta z)}\, e^{\eta t}, \quad \tilde{P} = f(x)\, e^{i(\alpha y + \beta z)}\, e^{\eta t}. \quad (16)$$

A wave vector is defined as $\mathbf{k} = (0, \alpha, \beta)$, with $k = (\alpha^2 + \beta^2)^{1/2}$ expressing the wave number. The complex parameter η utilised in Eq. (16) is such that its real part, q, is the exponential growth rate of the normal mode, while its imaginary part is $-\omega$, where ω is the angular frequency. The special cases $\alpha = 0$ and $\beta = 0$ yield the longitudinal rolls and the transverse rolls, respectively. A continuous change between these extrema can be parametrised as

$$\alpha = \sqrt{s}\, k, \quad \beta = \sqrt{1-s}\, k, \quad \text{with} \quad 0 \leqslant s \leqslant 1, \quad (17)$$

thus defining the oblique rolls when $0 < s < 1$, longitudinal rolls when $s = 0$, and transverse rolls when $s = 1$.

The transition to instability occurs when q changes from negative to positive values, so that the neutral stability condition is for $q = 0$. We now substitute Eq. (16) into Eqs. (15) and adopt the shorthand notation $D = d/dx$, so that we are led to an ordinary differential eigenvalue problem, namely

$$D\left[(1 + \xi|v_b|)^{-1} Df\right] - sk^2 (1 + 2\xi|v_b|)^{-1} f$$
$$- (1-s)k^2 (1 + \xi|v_b|)^{-1} f$$
$$- i\sqrt{s}\, k\, (1 + 2\xi|v_b|)^{-1} h = 0, \quad (18a)$$
$$D^2 h - \left(k^2 + \eta + i\sqrt{s}\, k v_b\right) h$$
$$+ R(1 + \xi|v_b|)^{-1} Df = 0, \quad (18b)$$
$$x = \pm 1/2: \quad f = 0, \quad h = 0. \quad (18c)$$

A. Longitudinal rolls

When our goal is the study of longitudinal rolls, then Eqs. (18) are simplified by setting $s = 0$,

$$D\left[(1 + \xi|v_b|)^{-1} Df\right] - k^2 (1 + \xi|v_b|)^{-1} f = 0, \quad (19a)$$
$$D^2 h - \left(k^2 + \eta\right) h + R(1 + \xi|v_b|)^{-1} Df = 0, \quad (19b)$$
$$x = \pm 1/2: \quad f = 0, \quad h = 0. \quad (19c)$$

We can gain some substantial information about these modes with an integral formulation. This means multiplying Eq. (19a) by $\bar{f}$, *viz.* the complex conjugate of f, integrating by parts over $-1/2 < x < 1/2$, and finally employing the boundary conditions (19c).

$$\int_{-1/2}^{1/2} (1 + \xi|v_b|)^{-1} |Df|^2\, dx$$
$$+ k^2 \int_{-1/2}^{1/2} (1 + \xi|v_b|)^{-1} |f|^2\, dx = 0. \quad (20)$$

With an arbitrary positive wave number, Eq. (20) happens to be satisfied only when f is identically zero. Thus if we set $f = 0$ in Eq. (19b), we can write

$$D^2 h - \left(k^2 + \eta\right) h = 0,$$
$$x = \pm 1/2: \quad h = 0. \quad (21)$$

Non-vanishing solutions of Eq. (21) are allowed if and only if

$$k^2 + \eta = -n^2 \pi^2, \quad n = 1, 2, 3, \ldots, \quad (22)$$

and they can be expressed as

$$h = A \sinh \left[\sqrt{k^2 + \eta} \left(x + \frac{1}{2} \right) \right], \qquad (23)$$

where an integration constant A has been employed. We recall that $\eta = q - i\omega$. Thus, Eq. (22) implies that $\omega = 0$. Furthermore, one has $q < 0$. Therefore, we conclude that the longitudinal rolls are linearly stable.

B. The limiting case of Darcy's flow

By setting $\xi \to 0$, we study the regime where the quadratic form–drag term is negligible and Darcy's law holds. In this limiting case, the basic velocity profile given by Eq. (7) becomes linear with $v_b = Rx$, and Eqs. (18) simplify to

$$D^2 f - k^2 f - i\sqrt{s} kh = 0,$$
$$D^2 h - \left(k^2 + \eta + i\sqrt{s} kRx \right) h + RDf = 0,$$
$$x = \pm 1/2 : \qquad f = 0, \qquad h = 0. \qquad (24)$$

This, then, is the regime analysed in the study by Barletta[6] and, in fact, Eq. (24) is identical to the eigenvalue stability problem studied in that paper.

V. NUMERICAL SOLUTION OF THE STABILITY PROBLEM

For general normal modes, $0 \leqslant s \leqslant 1$, Eqs. (18) can be solved numerically. There exist several different techniques which can be employed in the solution of the eigenvalue problems arising in the stability analyses of flows. A thorough and insightful review of such techniques can be found in chapter 19 of the book by Straughan[24]. Hereafter, we will base our analysis on the use of the shooting method. This method relies on a numerical solver of initial value problems, that is employed to evaluate the numerical solution (f, h) starting from one of the bounds of the interval $-1/2 \leqslant x \leqslant 1/2$, say the lower one, $x = -1/2$. Then, the conditions at the other bound, say the upper one, $x = 1/2$, are imposed for closing the solution and for evaluating the eigenvalues. In fact, one can manage Eqs. (18) as an eigenvalue problem due to their homogeneous nature. Which parameters are to be intended as the eigenvalues of the differential problem is, to a large extent, an arbitrary choice.

The linear system of differential equations (18) can be intended as an initial value problem provided that the boundary conditions at $x = -1/2$ are formally completed, namely

$$f(-1/2) = 0, \qquad f'(-1/2) = \chi_1 + i\chi_2,$$
$$h(-1/2) = 0, \qquad h'(-1/2) = 1. \qquad (25)$$

Here, setting $h'(-1/2) = 1$ is a way to break the scale–invariance of the homogeneous problem and to determine uniquely the eigenfunctions (f, h). The parameters χ_1 and χ_2 are unknowns and just represent the arbitrary real part and imaginary part of $f'(-1/2)$. Their values have just a mathematical meaning within the shooting method, but they are devoid of any physical implication. In fact, χ_1 and χ_2 are determined by the condition for breaking the scale invariance, in our case $h'(-1/2) = 1$. Hence, their values have just the same degree of arbitrariness as the scale–invariance breaking condition. The shooting method can be implemented by separating the parameters appearing in Eqs. (18) and (25) into two categories: input data and eigenvalues. As stated above, this distinction is mainly a matter of choice. We will adopt the scheme

$$\begin{cases} \text{input data:} & s, q, k, \xi, \\ \text{eigenvalues:} & R, \omega, \chi_1, \chi_2. \end{cases} \qquad (26)$$

The eigenvalues are obtained through a root finding technique, such as the Newton–Raphson method, employed to solve the target conditions,

$$f(1/2) = 0, \qquad h(1/2) = 0. \qquad (27)$$

The eigenvalues in Eq. (26) are given by real numbers whereas the target conditions in Eq. (27) yield complex equations. This is the reason why there are four (real) eigenvalues and just two (complex) target conditions.

The initial–value problem solver and the root finding method are implemented within the *Mathematica* (© Wolfram Research) software environment, through a script based on the use of functions NDSolve and FindRoot[25].

Table I serves to test the numerical accuracy of the finding root procedure for solving the stability eigenvalue problem (18). The test is a check of convergence for the fourth–order Runge–Kutta solver implemented through the *Mathematica* function NDSolve. The fixed step–size option is implemented with $\delta x = 10^{-N}$, and N increasing from 2 to 4 in steps of 0.2. The ultimate comparison is between the eigenvalues $R, \omega, \chi_1, \chi_2$ obtained with $\delta x = 10^{-4}$ and those computed by employing the adaptive step–size option. The discrepancy between the values of R is less than $6 \times 10^{-6}\,\%$, that regarding χ_1 is less than $8 \times 10^{-4}\,\%$ for χ_1, and that for χ_2 is less than $5 \times 10^{-4}\,\%$. The data for ω delineate a situation where, as $\delta x \to 0$, the angular frequency tends to zero. This is, in fact, the case for all the neutral stability data reported in this study. These findings imply that the transition from linear stability to instability is triggered by stationary normal modes. The convergence of ω to zero is oscillatory, with oscillations around zero of decreasing amplitude. On the other hand, the parameters accounted for in Table I undergo a monotonic convergence. This feature yields an apparent slower convergence of ω. However, one cannot judge the convergence rate from a single parameter as the convergence is relative to the whole solution and, hence, to the whole set of eigenvalues, as well as to the eigenfunctions.

The conclusion we draw from the data reported in Table I is that the fixed–step size algorithm is a satisfactory implementation of the Runge–Kutta solver and, thus, it is employed in all the results discussed hereafter.

TABLE I. Oblique rolls with $s = 0.5$, $k = 1$, $\xi = 0.01$: comparison between the neutral stability values of $(R, \omega, \chi_1, \chi_2)$ obtained by a fixed step–size Runge–Kutta solver having gradually decreasing step–size, $\delta x = 10^{-N}$, with an adaptive step–size Runge–Kutta solver

| N	R	ω	χ_1	χ_2
2.0	574.1487250	0.04503138296	0.02467819404	-0.02698728304
2.2	574.1418746	0.01706300442	0.02467057185	-0.02698226496
2.4	574.1168419	0.01122028490	0.02466927057	-0.02698158035
2.6	574.1294156	-0.00742607738	0.02466398575	-0.02697797823
2.8	574.1257225	-0.00099288777	0.02466580072	-0.02697921064
3.0	574.1273572	0.00453439813	0.02466730147	-0.02698019606
3.2	574.1269008	-0.00099909809	0.02466578455	-0.02697919140
3.4	574.1271954	0.00113458682	0.02466636797	-0.02697957693
3.6	574.1270999	0.00026781778	0.02466613067	-0.02697941994
3.8	574.1271471	-0.00028493251	0.02466597801	-0.02697931817
4.0	574.1271384	0.00045379328	0.02466618136	-0.02697945334
Adaptive	574.1271085	-0.00017646296	0.02466600834	-0.02697933857
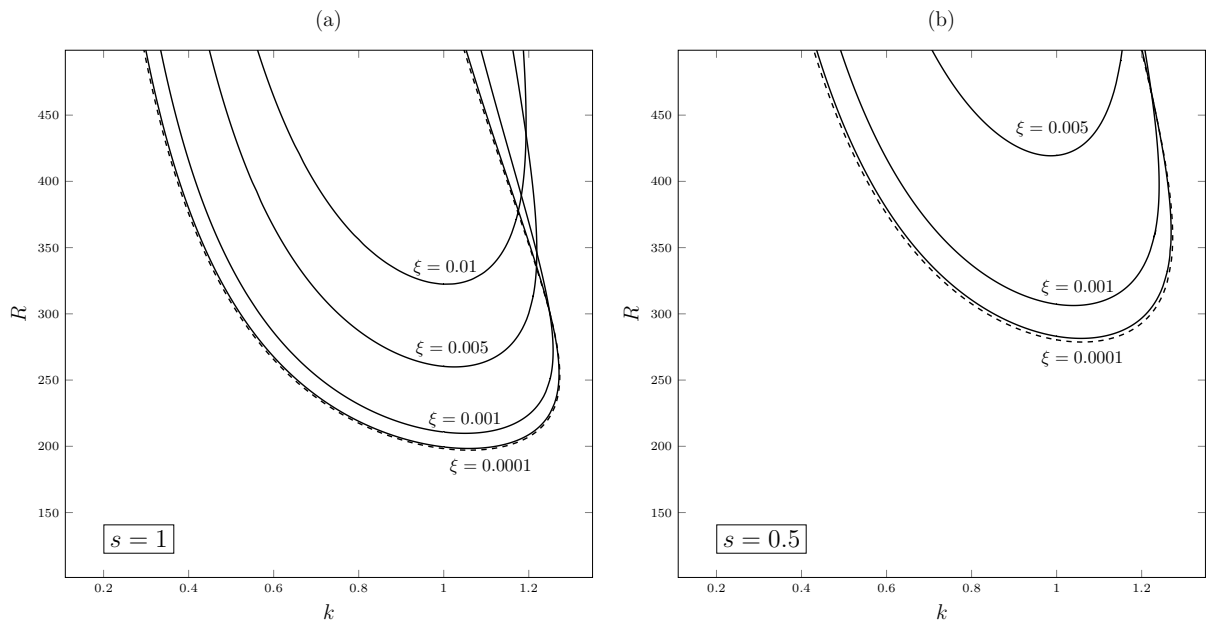
FIG. 3. Plots of the neutral stability curves, R versus k: (a) for transverse rolls ($s = 1$); (b) oblique rolls with $s = 0.5$. The limiting case of Darcy's law is denoted by dashed lines

VI. DISCUSSION OF THE RESULTS

The neutral stability condition ($q = 0$) is the bulk of a linear stability analysis as it provides the threshold between linear stability and instability. The graphical way to convey this information is by drawing a curve in the parametric plane (k, R) with the data obtained by solving for input values (s, q, k, ξ), where $q = 0$. This allows one to obtain the eigenvalues and, in particular, R. The point of minimum R along this curve yields the critical condition for the onset of instability. This means a pair (k_c, R_c) defining the critical wave number, k_c, and the critical Darcy–Rayleigh number, R_c. For $R < R_c$, no modal linear instability is possible. Thus, a larger R_c means a more linearly stable situation. The adjective "modal" employed here is important as, generally speaking, it has been

reported the possibility of non–modal linear instability occurring at subcritical conditions, $R < R_c$. An interesting survey on this topic can be found in Schmid[26].

Figure 3(a) shows the neutral stability curves for transverse rolls, while Fig. 3(b) is relative to oblique rolls with $s = 0.5$. For such oblique rolls, the angle between the wave vector and the vertical is $\pi/4$. In each case, different values of ξ are considered. The minimum of these curves moves upward as ξ increases and this implies a stabilising effect of the quadratic form–drag contribution to momentum transfer. In Figs. 3(a) and 3(b), dashed lines are reported denoting the limiting case where Darcy's law holds ($\xi \to 0$). A comparison between Figs. 3(a) and 3(b) reveals that, for a given ξ, oblique rolls with $s = 0.5$ are more stable than transverse rolls. We point out that the curve addressing the case with $s = 0.5$ and $\xi =$
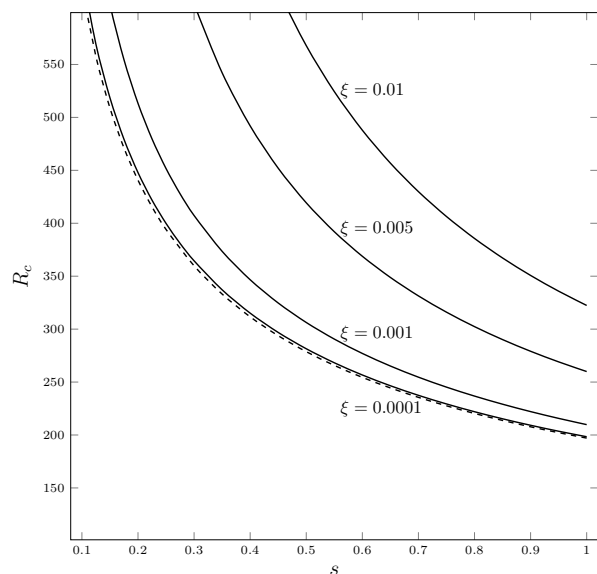
FIG. 4. Plots of R_c versus s for different ξ. The limiting case of Darcy's law is denoted by a dashed line

TABLE II. Transverse rolls $(s = 1)$: critical values of R and k for different ξ

ξ	R_c	k_c
0	197.081	1.05950
10^{-6}	197.094	1.05949
10^{-5}	197.209	1.05939
0.0001	198.359	1.05846
0.001	209.796	1.05007
0.005	259.937	1.02492
0.01	322.368	1.00687
0.02	448.012	0.98755

0.01 lies above the range of R considered in Fig. 3 and, thus, it is not displayed. All the neutral stability curves displayed in Fig. 3 manifest the same important feature pointed out by Barletta [6] for the case $\xi \to 0$. Along the neutral stability curve, there exists a point of maximum k delimiting the region where linear instability is possible.

Figure 4 clearly establishes the feature suggested by Fig. 3. This figure shows that R_c is a monotonically decreasing function of s or, stated differently, that transverse rolls $(s = 1)$ are the most unstable modes. This is an extremely important fact as we are motivated, in the following, to focus our study of the onset of linear instability to transverse rolls. The range considered in Fig. 4 is $0.1 < s \leqslant 1$, due to the singularity of R_c when $s \to 0$. This singularity is a further evidence that longitudinal rolls $(s = 0)$ never lead to instability.

Figure 5 is relative to transverse rolls, *viz.* the most unstable modes of perturbation. The trends of R_c and k_c versus ξ are displayed on a logarithmic scale for ξ, which amplifies the behaviour at smaller values of the form–drag number and evidences the asymptotic regime of Darcy's flow happening when $\xi \to 0$. On one hand, Fig. 5 shows the stabilising role

of the form–drag effect, as R_c increases monotonically with ξ. On the other hand, this figure points out that the quadratic form-drag term implies that the onset of instability involves smaller and smaller wave numbers, as k_c is a monotonic decreasing function of ξ. All these features are perfectly coherent with the plots of the neutral stability curves represented in Fig. 3(a).

Some computed values of R_c and k_c with six significant figures are presented in Table II. The computations have been done for some values of ξ, while the case $\xi = 0$ serves for comparison. The values of R_c and k_c for this case coincide perfectly with those reported by Barletta [6] for the Darcy's law limit.

Plots of the perturbation streamlines and isotherms in the xy plane for transverse rolls $(s = 1)$ are displayed in Fig. 6. In this figure, a comparison is made between two utterly different cases, namely the onset conditions for instability (α_c, R_c) with either $\xi = 0$ or $\xi = 0.05$. The qualitative differences emerging in these two very dissimilar flow regimes are not as large as expected. In fact, there is a very marked gap between the values of R_c and $\xi = 0.05$ is an extremely large form–drag number. An evident feature of the convection cells is that they are open to the external environment with a continuous inflow/outflow at the boundaries. This behaviour is a consequence of the permeable nature of the planes $z = -1/2$ and $z = 1/2$ and of the isobaric conditions imposed.

VII. CONCLUSIONS

Free convection in a vertical porous slab has been analysed. The plane and parallel vertical boundaries have been modelled as isothermal and open to external quiescent fluid reservoirs, thus leading to uniform temperature and pressure boundary conditions. The momentum transfer for the fluid saturating the porous medium has been described through the Darcy–Forchheimer law by assuming an important contribution of the quadratic form–drag effect. The form–drag number, ξ, has been included among the governing dimensionless parameter, together with the Darcy–Rayleigh number, R, which is a measure of the intensity of the buoyancy force caused by the unequal boundary temperatures. We proved that there exists a stationary basic flow with a parallel vertical velocity field and a purely transverse temperature gradient. The temperature distribution across the slab displays a departure from the linear due to the form–drag effect.

The linear instability of the basic flow has been studied. General normal modes of perturbation have been considered, oriented in all possible directions parallel to the boundary planes. The local balance equations of mass, momentum and energy led us to the formulation of an ordinary differential eigenvalue problem. The main features of the instability analysis are the following:

- For the special case of longitudinal rolls, *viz.* the normal modes with a horizontal wave vector, it has been proved that no instability exists.

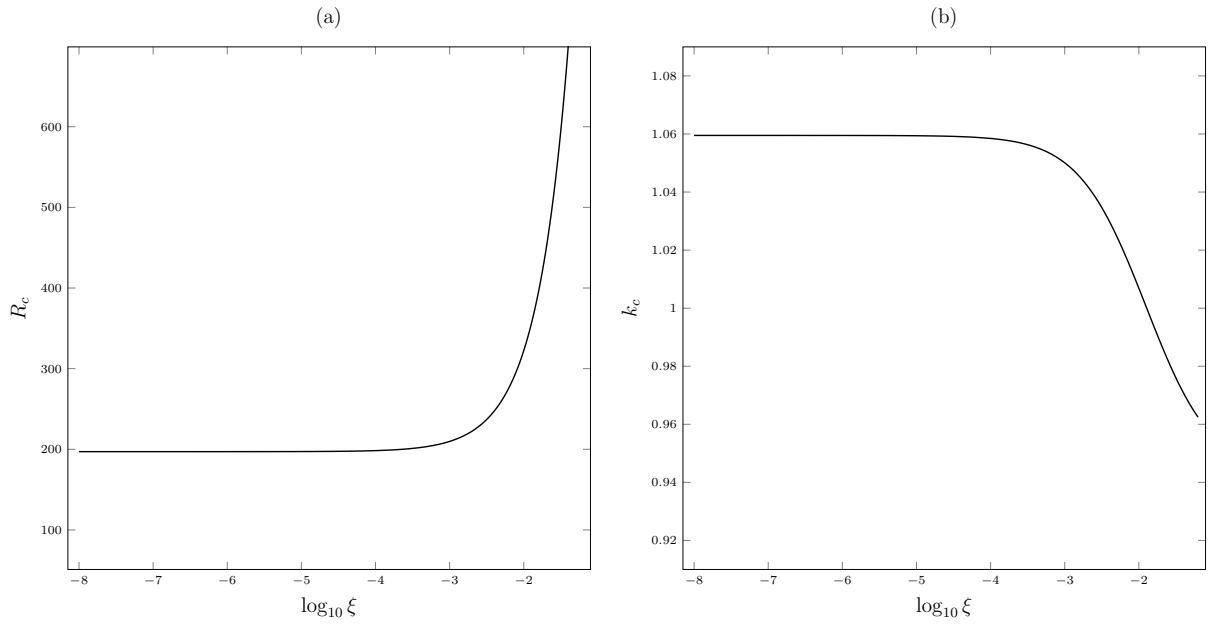- For the general case, the solution of the instability

FIG. 5. Transverse rolls ($s = 1$): (a) plot of R_c versus ξ; (b) plot of k_c versus ξ

$\xi = 0, \quad s = 1,$
$k_c = 1.05950, \quad R_c = 197.081$

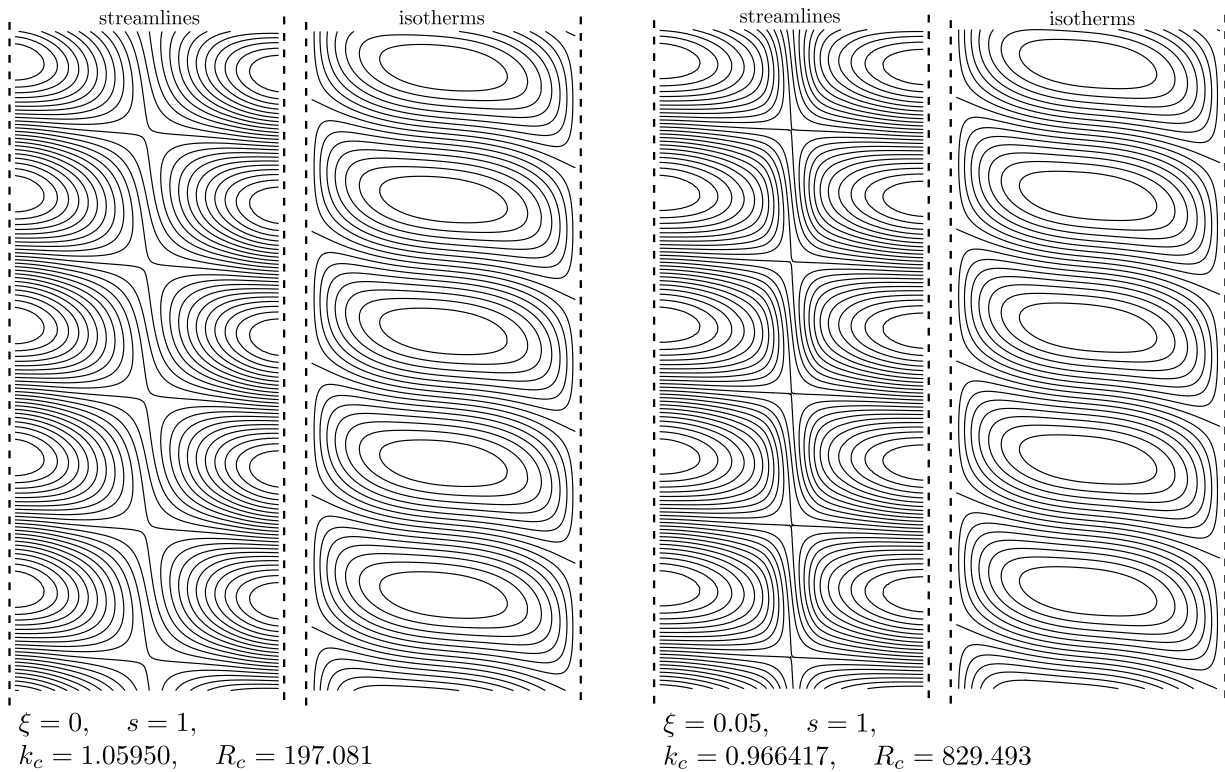$\xi = 0.05, \quad s = 1,$
$k_c = 0.966417, \quad R_c = 829.493$

FIG. 6. Streamlines and isotherms in the xy plane for the perturbation flow at critical conditions with $s = 1$ and either $\xi = 0$ or $\xi = 0.05$

eigenvalue problem has been carried out numerically by utilising the shooting method and a Runge–Kutta solver. This solution allowed us to conclude that the transverse rolls, *viz.* the normal modes with a vertical wave vector, yield the lowest possible values of R at on-set of instability. In other words, the transverse rolls are the most unstable modes of perturbation.

- The quadratic form–drag effect yields a stabilisation of the basic flow. The Darcy's law limit, $\xi \to 0$, represents the term of comparison for this conclusion. In fact, the

neutral stability condition for transverse rolls yields a critical value of R monotonically increasing with the form–drag number ξ.

- The neutral stability curves drawn in the $(k, R)-$plane, where k is the wave number, illustrate a situation where no linear instability emerge when k exceeds a maximum threshold. Such a threshold wave number undergoes a change with the form–drag number ξ.

Several perspectives of future developments for this study can be envisaged. Among them, a weakly nonlinear stability analysis may be very important both for the supercritical and the subcritical parametric regime. One can gain important information regarding the heat transfer rates across the porous slab when the convective rolls break the conduction regime. It would also be interesting to study the stability of the bifurcated flow to analyse the appearance of periodic oscillations and their impact on the heat transfer. On the other hand, one can inspect the possible existence of a subcritical instability which cannot be excluded by the present analysis.

[1] K. Boomsma, D. Poulikakos, and F. Zwick, "Metal foams as compact high performance heat exchangers," Mechanics of Materials **35**, 1161–1176 (2003).

[2] D. A. Nield and A. Bejan, *Convection in Porous Media*, 5th ed. (Springer-Verlag, New York, 2017).

[3] A. E. Gill, "A proof that convection in a porous vertical slab is stable," Journal of Fluid Mechanics **35**, 545–547 (1969).

[4] B. Straughan, "A nonlinear analysis of convection in a porous vertical slab," Geophysical & Astrophysical Fluid Dynamics **42**, 269–275 (1988).

[5] J. N. Flavin and S. Rionero, "Nonlinear stability for a thermofluid in a vertical porous slab," Continuum Mechanics and Thermodynamics **11**, 173–179 (1999).

[6] A. Barletta, "A proof that convection in a porous vertical slab may be unstable," Journal of Fluid Mechanics **770**, 273–288 (2015).

[7] C. M. Vest and V. S. Arpaci, "Stability of natural convection in a vertical slot," Journal of Fluid Mechanics **36**, 1–15 (1969).

[8] S. A. Korpela, D. Gözüm, and C. B. Baxi, "On the stability of the conduction regime of natural convection in a vertical slot," International Journal of Heat and Mass Transfer **16**, 1683–1690 (1973).

[9] G. D. McBain and S. W. Armfield, "Natural convection in a vertical slot: accurate solution of the linear stability equations," The ANZIAM Journal **45**, C92–C105 (2004).

[10] M. S.-E. Imbabi, "Modular breathing panels for energy efficient, healthy building construction," Renewable Energy **31**, 729–738 (2006).

[11] A. Barletta and D. A. S. Rees, "Local thermal non-equilibrium analysis of the thermoconvective instability in an inclined porous layer," International Journal of Heat and Mass Transfer **83**, 327–336 (2015).

[12] M. Celli, A. Barletta, and D. A. S. Rees, "Local thermal non-equilibrium analysis of the instability in a vertical porous slab with permeable side-walls," Transport in Porous Media **119**, 539–553 (2017).

[13] A. Barletta, M. Celli, and M. Ouarzazi, "Unstable buoyant flow in a vertical porous layer with convective boundary conditions," International Journal of Thermal Sciences **120**, 427–436 (2017).

[14] P. Bera and M. K. Khandelwal, "A thermal non–equilibrium perspective on instability mechanism of non-isothermal Poiseuille flow in a vertical porous–medium channel," International Journal of Thermal Sciences **105**, 159–173 (2016).

[15] A. Barletta, "Instability of stationary two–dimensional mixed convection across a vertical porous layer," Physics of Fluids **28**, 014101 (2016).

[16] B. M. Shankar, J. Kumar, and I. S. Shivakumara, "Magnetohydrodynamic stability of natural convection in a vertical porous slab," Journal of Magnetism and Magnetic Materials **421**, 152–164 (2017).

[17] B. M. Shankar and I. S. Shivakumara, "On the stability of natural convection in a porous vertical slab saturated with an Oldroyd–B fluid," Theoretical and Computational Fluid Dynamics **31**, 221–231 (2017).

[18] A. Barletta and M. Celli, "Instability of parallel buoyant flow in a vertical porous layer with an internal heat source," International Journal of Heat and Mass Transfer **111**, 1063–1070 (2017).

[19] B. M. Shankar, J. Kumar, and I. S. Shivakumara, "Stability of natural convection in a vertical layer of Brinkman porous medium," Acta Mechanica **228**, 1–19 (2017).

[20] A. K. Sharma and P. Bera, "Linear stability of mixed convection in a differentially heated vertical channel filled with high permeable porous-medium," International Journal of Thermal Sciences **134**, 622–638 (2018).

[21] A. K. Sharma, M. K. Khandelwal, and P. Bera, "Finite amplitude analysis of non–isothermal parallel flow in a vertical channel filled with a highly permeable porous medium," Journal of Fluid Mechanics **857**, 469–507 (2018).

[22] D. A. S. Rees, "The effect of inertia on the onset of mixed convection in a porous layer heated from below," International Communications in Heat and Mass Transfer **24**, 277–283 (1997).

[23] A. Barletta and D. A. S. Rees, "Unstable mixed convection flow in a horizontal porous channel with uniform wall heat flux," Transport in Porous Media , doi: 10.1007/s11242–019–01294–y (in press).

[24] B. Straughan, *The Energy Method, Stability, and Nonlinear Convection*, 2nd ed. (Springer, New York, NY, 2004).

[25] Wolfram Research, Inc., "Mathematica, Version 11.3," `https://reference.wolfram.com/language/` (Champaign, IL, 2018).

[26] P. J. Schmid, "Nonmodal stability theory," Annual Review of Fluid Mechanics **39**, 129–162 (2007).